Matters Arising

Cell

No Evidence for Cardiomyocyte Number Expansion in Preadolescent Mice

Graphical Abstract

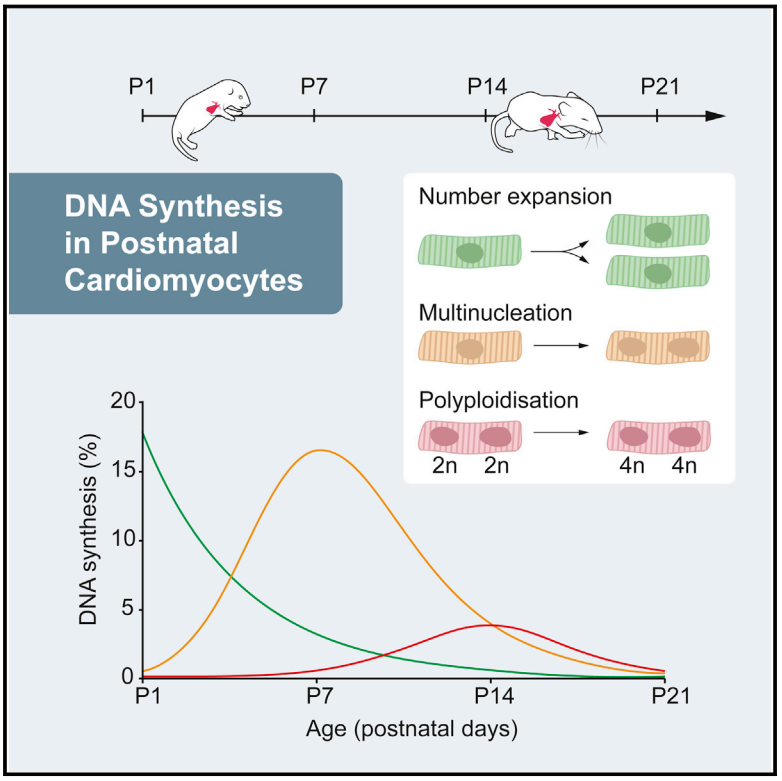

Authors

Kanar Alkass, Joni Panula, Mattias Westman, Ting-Di Wu, Jean-Luc Guerquin-Kern, Olaf Bergmann

Correspondence

olaf.bergmann@ki.se

In Brief

Contrary to a recent report suggesting that a preadolescent burst of cardiomyocyte proliferation promotes heart growth, cardiomyocyte number expansion appears limited to the neonatal period, with cardiomyocyte hypertrophy likely accounting for the increase in the heart size.

Highlights

- Cardiomyocyte number expansion is limited to the neonatal period
- Multinucleation and ploidisation follow neonatal cardiomyocyte duplication
- Cardiomyocyte hypertrophy is sufficient to explain preadolescent heart growth

Alkass et al., 2015, Cell *163*, 1026–1036
November 5, 2015 ©2015 Elsevier Inc.
http://dx.doi.org/10.1016/j.cell.2015.10.035

Cell

Matters Arising

No Evidence for Cardiomyocyte Number Expansion in Preadolescent Mice

Kanar Alkass,[1,2] Joni Panula,[1] Mattias Westman,[3] Ting-Di Wu,[4,5] Jean-Luc Guerquin-Kern,[4,5] and Olaf Bergmann[1,*]
[1]Cell and Molecular Biology, Karolinska Institutet, SE-17177 Stockholm, Sweden
[2]Department of Forensic Medicine, The National Board of Forensic Medicine, SE-17177 Stockholm, Sweden
[3]Department of Medicine, Karolinska Institutet, SE-14186 Huddinge, Sweden
[4]Institut Curie, Centre de Recherche, F-91405 Orsay, France
[5]INSERM, U1196; CNRS, UMR9187, F-91405 Orsay, France
*Correspondence: olaf.bergmann@ki.se
http://dx.doi.org/10.1016/j.cell.2015.10.035

SUMMARY

The magnitude of cardiomyocyte generation in the adult heart has been heavily debated. A recent report suggests that during mouse preadolescence, cardiomyocyte proliferation leads to a 40% increase in the number of cardiomyocytes. Such an expansion would change our understanding of heart growth and have far-reaching implications for cardiac regeneration. Here, using design-based stereology, we found that cardiomyocyte proliferation accounted for 30% of postnatal DNA synthesis; however, we were unable to detect any changes in cardiomyocyte number after postnatal day 11. ^{15}N-thymidine and BrdU analyses provided no evidence for a proliferative peak in preadolescent mice. By contrast, cardiomyocyte multinucleation comprises 57% of postnatal DNA synthesis, followed by cardiomyocyte nuclear polyploidisation, contributing with 13% to DNA synthesis within the second and third postnatal weeks. We conclude that the majority of cardiomyocytes is set within the first postnatal week and that this event is followed by two waves of non-replicative DNA synthesis. This Matters Arising paper is in response to Naqvi et al. (2014), published in *Cell*. See also the associated Correspondence by Soonpaa et al. (2015), and the response by Naqvi et al. (2015), published in this issue.

INTRODUCTION

The replacement of cardiomyocytes has been a major challenge in regenerative medicine. The neonatal mouse heart exhibits robust myogenesis after apical resection and ischemic lesions; this myogenesis is mainly mediated by duplication of preexisting cardiomyocytes (Ali et al., 2014; Porrello et al., 2011; Puente et al., 2014), although there is also evidence for a contribution of precursor cells (c-kit-positive) to the regenerating myocardium (Jesty et al., 2012). This regenerative process seems to be limited to the first postnatal week (Puente et al., 2014), which coincides with an increase in binucleation in cardiomyocytes (Soonpaa et al., 1996; Walsh et al., 2010). Senyo et al. evaluated the degree of cardiomyocyte proliferation via the detection of the non-radioactive isotope ^{15}N-thymidine in dividing cardiomyocytes. They observed limited myogenesis in both young and old mice, with annual proliferation rates of less than 1% (Senyo et al., 2013), in agreement with the human cardiomyocyte renewal rates established by ^{14}C birth dating (Bergmann et al., 2009; 2015)

In contrast to these findings, Naqvi et al. (2014) reported a second wave of cardiomyocyte proliferation during preadolescence that occurs in a highly synchronized fashion. Most cardiomyocytes re-entered the cell cycle starting on the evening of postnatal day 14, followed by mitosis and cytokinesis on postnatal day 15. This proliferative event remarkably increased the cardiomyocyte count by 40%. As most cardiomyocytes are binucleated at this stage, the authors suggested a model in which binucleated cardiomyocytes undergo karyokinesis, resulting in tetranucleated cardiomyocytes, followed by cytokinesis to generate two mononucleated cardiomyocytes and one binucleated cardiomyocyte. These replicative events were suggested to be mediated by thyroid hormone (T3) through the IGF-1/Akt pathway. These observations were provocative because another recent study demonstrated that the increase in oxygen at birth induces DNA damage, leading to cell-cycle arrest in cardiomyocytes shortly after birth (Puente et al., 2014). The findings reported by Naqvi et al. suggest a more complex regulation of cardiomyocyte proliferation and consequently have major implications for the understanding of cardiomyocyte proliferation (Palpant and Murry, 2014; Zhang and Kühn, 2014). We have re-examined their key observations, using both similar and alternative approaches. We observed that cardiomyocyte expansion is restricted mainly to the first postnatal week, seriously challenging the reported contribution of cardiomyocyte proliferation to the growing preadolescent mouse heart. Instead, we observed that, in addition to multinucleation, murine cardiomyocytes undergo polyploidization in the second and third postnatal weeks. This time period corresponds well to the increase in ploidy in human preadolescent hearts (Bergmann et al., 2009; Mollova et al., 2013). This study also supports recent reports of substantial early postnatal cardiomyogenesis without finding any evidence for a second wave of cardiomyocyte proliferation contributing to heart growth.

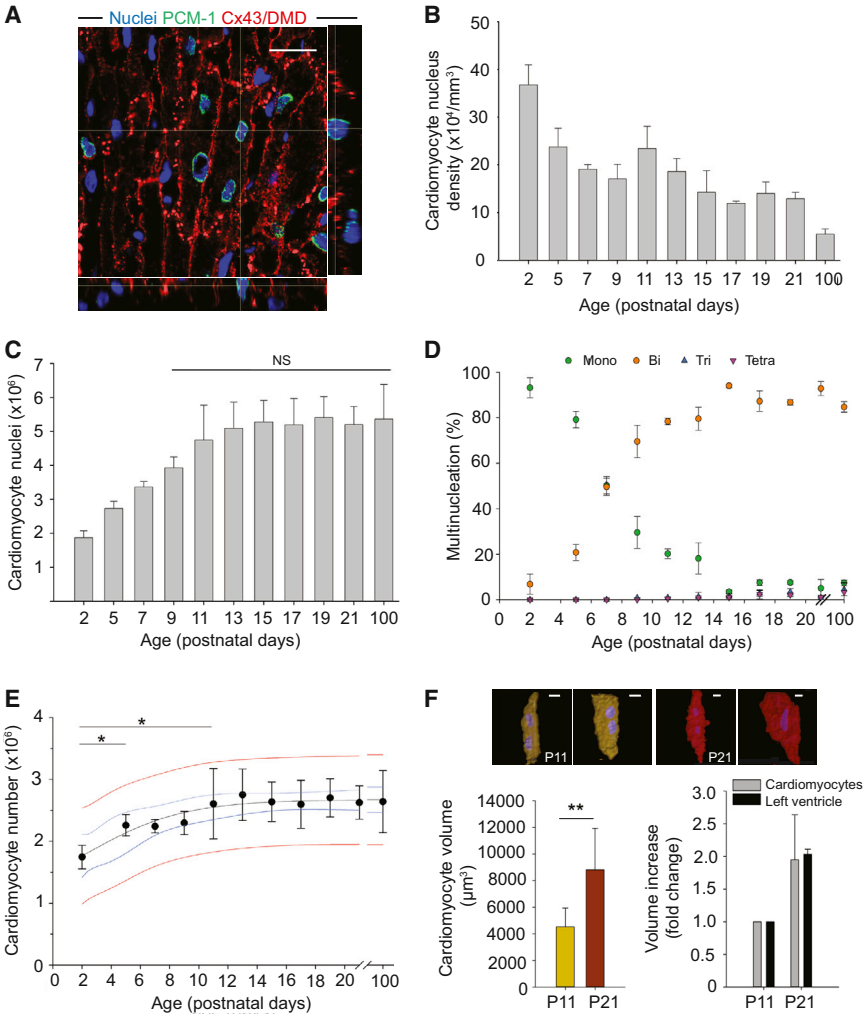

Figure 1. Expansion of the Pool of Cardiomyocytes in Neonatal Mouse Hearts

(A) The labeling strategy used to unequivocally identify cardiomyocyte nuclei and the number of nuclei per cardiomyocyte. Cardiomyocyte nuclei were labeled with antibodies against PCM-1 (green), and the cardiomyocyte cell borders were labeled with antibodies against connexin43 (Cx43) and dystrophin (DMD) (red). The scale bar indicates 20 μm.

(B) The cardiomyocyte density decreased during heart growth from P2 to P100.

(C) The number of cardiomyocyte nuclei plateaued around P11 and remained constant thereafter (n = 3 to 6 for all analyzed time points).

(D) The process of multinucleation began early in the neonatal period. At P9, most cardiomyocytes already contained two or more nuclei.

(E) Stereological analysis revealed that the number of cardiomyocytes increased in the early neonatal period from 1.7 × 10^6 on P2 to 2.26 × 10^6 on P5 and reach a plateau on P11 (95% confidence interval (blue), 95% prediction interval (red)).

(F) The results of the volume analysis of isolated cardiomyocytes on P11 and P21. The upper panel shows cardiomyocytes isolated on P11 (yellow) and P21 (red) rendered by the Imaris software to obtain their individual volumes (n = 3 for both groups, total of 274 cardiomyocytes analyzed). Scale bars,10 μm. Note the different lengths of the scale bars in the images of cardiomyocytes from P11 and P21. The left ventricle (black bars) increased 2.0-fold between P11 and P21, comparable to the increase in the average cardiomyocyte volume (gray bars) (right). * indicates $p < 0.05$; ** indicates $p < 0.001$; NS: not significant. All error bars indicate SD.

RESULTS

The Final Number of Cardiomyocytes Is Mainly Established within the First Postnatal Week

We determined the number of cardiomyocytes by stereology in mouse hearts from postnatal day 2 (P2) to postnatal day 100 (P100) (Figure 1). The identification of cardiomyocyte nuclei in tissue sections is challenging, particularly in the perinatal period when the cell density is very high (Ang et al., 2010; Soonpaa and Field, 1998). To circumvent this problem, we used antibodies against the cardiomyocyte nuclear marker pericentriolar material 1 (PCM-1) (Figure 1A) (Bergmann and Jovinge, 2012; Bergmann et al., 2011; Gilsbach et al., 2014). We obtained the mass of the left ventricle by weighting the left ventricle including the septum (Figures S1A and S1B). The reference volume was calculated using the tissue density of the myocardium (1.06 g/cm^3) (Brüel and Nyengaard, 2005). The density of myocyte nuclei gradually decreased from 367,504 ± 42,055/mm^3 (mean ± SD) on P2 to 128,983 ± 13,555/mm^3 on P20 and 55,085 ± 10,574/mm^3 on P100 (Figure 1B).

Next, we established the number of postnatal cardiomyocyte nuclei (Experimental Procedures). The number of cardiomyocyte nuclei expanded continuously between P2 (1.87 × 10^6 ± 0.20 × 10^6) and P11 and plateaued thereafter (4.75 × 10^6 ± 1.04) (ANOVA, post hoc Holm-Sidak, $p > 0.05$) (Figure 1C). The ratio of mono- to multinucleated cardiomyocytes changed substantially during the first 10 postnatal days. On P2, the majority (93.2% ± 4.4%) of cardiomyocytes remained mononucleated, in agreement with previous studies, whereas on P11, only 20.2% ± 2.2% were mononucleated, and 78.4% ± 1.5% were binucleated. We did not observe any further changes in this ratio between P11 and P100 (Figure 1D). Taking multinucleation into account, we established that cardiomyocytes expanded by approximately 40% between P2 (1.7 × 10^6 ± 0.2 × 10^6) and P5 (2.3 × 10^6 ± 0.2 × 10^6) (ANOVA, post hoc t test with Holm-Bonferroni correction, $p < 0.05$) and then plateaued on P11 (2.6 × 10^6 ± 0.6 × 10^6) and remained constant at least until P100 (linear regression, R = 0.016, p = 0.935, Figures 1E and S1C).

To investigate the contribution of the increase in cardiomyocyte volume to the preadolescent growth of the left ventricle (Leu et al., 2001), we determined the average volume of

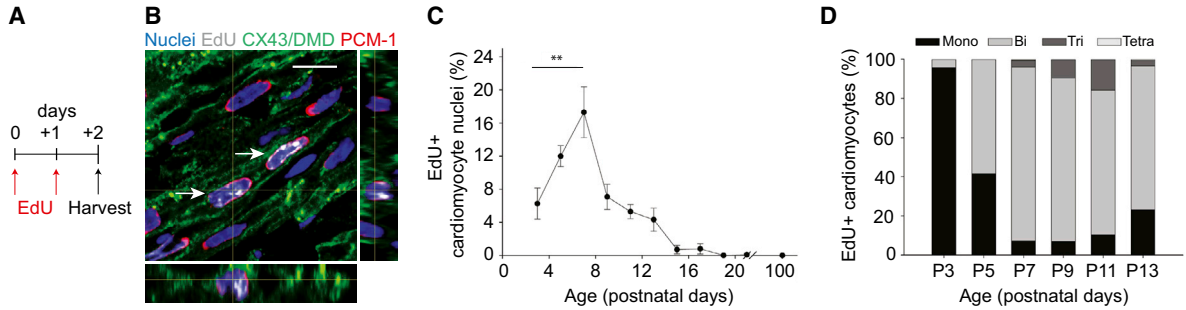

Figure 2. Cardiomyocyte DNA Synthesis in the Growing Mouse Heart

(A) Two EdU pulses were given on 2 consecutive days. Mice were sacrificed after a 24-hr chase period.

(B) EdU incorporation was detected in cardiomyocyte nuclei by co-labeling with PCM-1, and connexin43 (Cx43) and dystrophin (DMD) staining were used to delineate cell borders. Arrows indicate EdU-positive cardiomyocyte nuclei. The scale bars, 10 μm.

(C) The postnatal DNA synthesis in cardiomyocytes was highest in mice sacrificed on P7 (~17%), and rapidly declined thereafter to values below 1% on P15 (n = 3–4, for all analyzed time points).

(D) Mononucleated cardiomyocytes incorporated most of the EdU on P3, but by P7, most cardiomyocytes were bi- or multinucleated. The relative increase in the number of mononucleated EdU-positive cardiomyocytes on P13 may be related to the increase in nuclear ploidy (Figure 3). ** indicates $p < 0.001$.

All error bars indicate SD.

cardiomyocytes on day P11 (4,530 μm^3 ± 1,410 μm^3) and P21 (8,820 μm^3 ± 3,120 μm^3) (t test, $p < 0.01$) (Figure 1F and Experimental Procedures). We determined that the 2.0-fold increase in the volume of the left ventricle (P11: 20.1 ± 1.3 mm^3 and P21: 40.8 ± 1.6 mm^3) could be fully explained by the volume increase (2.0-fold) of cardiomyocytes, indicating mainly hypertrophic growth of the left ventricle and establishment of the full complement of cardiomyocytes by P11.

Postnatal DNA Synthesis Changes Mononucleated Cardiomyocytes into Multinucleated Cardiomyocytes

The mice were treated with the thymidine analog EdU on two consecutive days and sacrificed one day after the second treatment (Figure 2A). The frequency of EdU incorporation was determined by co-labeling with antibodies against cardiomyocyte nuclei (PCM-1) (Figures 2B and C). The EdU labeling frequency peaked on P7 (17.3% ± 3.1%) (ANOVA, $p < 0.001$, post hoc, Holm-Sidak, $p < 0.001$), followed by a continuous decline to ratios of less than 1% on P15. On P100, we identified only one EdU-labeled cardiomyocyte nucleus among 980 analyzed nuclei (Figure 2C). Next, we investigated the distribution of EdU incorporation into mono- and multinucleated cardiomyocytes (Figures 2B and 2D). In agreement with cardiomyocyte proliferation, EdU incorporation was predominantly observed in mononucleated cardiomyocytes on P3 (95.8% ± 1.9%) and rapidly changed during the first postnatal week (P7), when most EdU-labeled cardiomyocytes became binucleated (mononucleated: 7.3% ± 3.5%, binucleated: 88.7% ± 5.2%, and multinucleated: 4.0% ± 2.2%) (Figure 2D). Our data support a previous report suggesting an early postnatal switch from cardiomyocyte proliferation to multinucleation (Soonpaa et al., 1996; Walsh et al., 2010).

Cardiomyocyte DNA Content Increases during the Second and Third Postnatal Weeks

Many cardiomyocyte nuclei undergo DNA synthesis to become polyploid in humans (Adler, 1991; Bergmann et al., 2009; Herget et al., 1997; Mollova et al., 2013). However, ploidy changes in juvenile mouse hearts have not been systematically investigated. We therefore determined the DNA content of murine cardiomyocyte nuclei on different postnatal days by flow cytometry (Figures 3A to 3D, and S2). Most cardiomyocyte nuclei were diploid around birth until P9 (Figures 3C, left, and S2), corresponding to 104.7% ± 0.4% in Figure 3D. Between postnatal weeks 2 and 3, the average DNA content per nucleus increased by approximately 10% in the left ventricle (Figures 3C, right, and S2) to 115.5% ± 2.3% (Figure 3D, ANOVA $p < 0.001$) and remained constant thereafter until P100 (Figure 3D). This finding is also reflected by an increase in the ploidy of the EdU-labeled cardiomyocyte nuclei between P3 and P13 (Figures 3E and 3F).

Cardiomyocytes Exhibit No Enhanced Cell-Cycle Activity in Preadolescent Mice

Ki-67 is expressed in all phases of the cell cycle including mitotic events (Scholzen and Gerdes, 2000). Thus, we used Ki-67 to exclude substantial cell-cycle activity on P14 and P15 as described by Naqvi et al. (2014). We sacrificed postnatal mice on P14 at 9:00 p.m., on P15 at noon, and on P16 at 9:00 a.m. The shorter length of our analysis intervals (14 hr and 21 hr) compared to the average mammalian cell-cycle length of approximately 24 hr (Hahn et al., 2009; Ponti et al., 2013) would allow us to detect any cell-cycle activity on P15. However, we could not detect any significant difference between P14, P15, and P16 (Holm-Sidak method, $p > 0.05$). By contrast, we observed that these three time points all exhibited Ki-67 frequencies of less than 2% compared to that on P7 (ANOVA, $p < 0.001$) (Figures 4A and 4B).

PCM-1 disassembles in pro-metaphase and metaphase of mitosis (Srsen et al., 2009). Although PCM-1 can be detected in all other phases of the cell cycle, we excluded the possibility that we underestimated the number of cycling cardiomyocytes by also using antibodies against cardiac troponin I to identify cardiomyocyte nuclei by their location in the cardiomyocyte cytoplasm (Figure 4B).

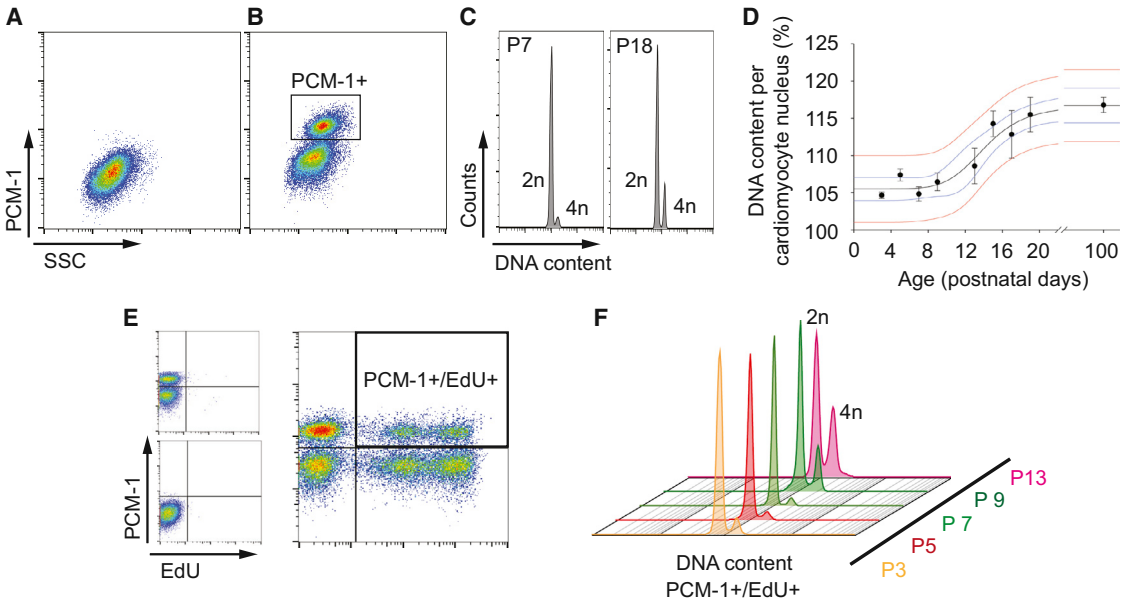

Figure 3. Cardiomyocyte Nuclear Ploidy in the Growing Mouse Heart

(A and B) Cardiomyocyte nuclei were labeled with isotype controls (A) and antibodies against PCM-1 (B).

(C) Two representative flow cytometry histograms depict the DNA content of cardiomyocyte nuclei (PCM-1-positive) from P7 and P18 mice.

(D) Time course of the cardiomyocyte DNA content per nucleus. Cardiomyocyte nuclei undergo polyploidization during the second and third postnatal weeks (95% confidence interval [blue], 95% prediction interval [red]; 100% corresponds to a pure diploid population [2n], and 200% to a pure tetraploid population [4n]).

(E and F) Flow cytometric analysis of the EdU-positive cardiomyocyte nuclear ploidy (see Figure 2A for the time course of EdU injection). (E) Representative flow cytometry plots for immunolabeling of P7 animals with antibodies against PCM-1 and EdU detection (PCM-1+/EdU+). Note that the different fluorescent intensities within the EdU-positive populations indicate different levels of EdU incorporation. Cells may have gone through the S-phase twice after BrdU was delivered. Lower left: flow cytometry plots with isotype control antibodies and without EdU detection; upper left: flow cytometry plots with PCM-1 antibodies and without EdU detection.

(F) The nuclear ploidy of EdU-positive cardiomyocyte nuclei measured at different time points (P3 to P13). The nuclear ploidy began to increase on P9. 2n: diploid; 4n: tetraploid; SSC: side scatter.

All error bars indicate SD.

BrdU Incorporation Reveals Only Minimal DNA Synthesis in Preadolescent Cardiomyocytes

Naqvi et al. proposed a highly synchronized last round of cardiomyocyte proliferation beginning on the evening of P14. Thymidine analogs such as BrdU have a short biological half-life. Therefore, it might be difficult to detect the suggested cardiomyocyte DNA synthesis on P15 with a single BrdU injection. Consequently, we subcutaneously implanted a pellet on P13 that continuously released BrdU (Experimental Procedures and Figures 4C to 4I). BrdU incorporation into cardiomyocyte nuclei (PCM-1-positive) was detected by immunohistochemistry (IHC) (Figures 4D and 4E) and flow cytometry on P18 (Figures 4F to 4H). Both experimental strategies revealed a BrdU incorporation rate of less than 3% in cardiomyocyte nuclei (IHC: 1.8% ± 0.9%; flow cytometry: 2.9% ± 1.4%) (Figure 4I). An analysis of the DNA content in BrdU-positive nuclei revealed an increase in nuclear ploidy in cardiomyocytes compared to non-cardiomyocytes (Figure 4H). These findings exclude the possibility of a major proliferative cardiomyocyte burst between P13 and P18. By contrast, the majority of BrdU-positive cardiomyocyte nuclei were tetraploid, indicating that DNA synthesis is linked to polyploidization rather than proliferation after P13 (also see Figure 3). Furthermore, we did not observe any differences in the BrdU labeling frequency of endocardial (1.4% ± 0.4%) or epicardial cardiomyocyte (1.3% ± 0.6%) nuclei (paired t test, p = 0.93) (Figures 4D and S3).

Multi-Isotope Mass Spectrometry Analyses of 15N Thymidine Incorporation Provide No Evidence of a Second Wave of Cardiomyocyte Proliferation in Preadolescent Mice

We continuously administered 15N-thymidine (Experimental Procedures) in preadolescent mouse hearts (P13–P23) (Figure 5A) to exclude the possibility that continuous delivery of the halogenated thymidine analogs (BrdU or EdU) might be associated with toxic effects that alter cell turnover (Andersen et al., 2013; Wilson et al., 2008). Nonradioactive stable isotope tracers such as 15N-thymidine do not alter biochemical reactions and are not harmful to the animal (Steinhauser et al., 2012). Multi-isotope imaging mass spectrometry (MIMS) allows the simultaneous detection of the stable isotopes of the same element (Senyo et al., 2013). Due to the low natural abundance of 15N (0.37%), the incorporation of a 15N-labeled tracer is readily detected due to an increase in the 15N:14N ratio. Because DNA contains a high amount of phosphate, we also visualized phosphorus (31P) in addition to the 15N:14N ratio to identify cardiac nuclei with high spatial resolution (Figures 5B to 5D). At a lateral resolution of less than 100 nm,

cardiomyocytes were identified based on the cell borders and their subcellular specific ultrastructure, allowing the identification of cardiomyocyte nuclei based on their location (Figures 5B to 5D). The nuclear 15N integration was evenly distributed throughout the investigated myocardium (Figure S4). In addition to analyzing 15N thymidine incorporation on sections, we isolated cardiomyocyte nuclei by flow cytometry (as shown in Figure 3A and 3B), and determined 15N thymidine incorporation subsequently (Figure 5E). In both experimental designs we observed 15N-thymidine incorporation in only a small fraction of cardiomyocyte nuclei between P13 and P23 (0.9% to 2.1%) (t test, $p > 0.05$) (Figures 5B to 5F), comparable to the data obtained by BrdU infusion (Figures 4C to 4I) and not compatible with the robust cardiomyocyte proliferation suggested by Naqvi et al.

An Integrated Model of DNA Synthesis in Postnatal Cardiomyocytes

Based on our data obtained by design-based stereology (Figures 1A to 1E) and by flow cytometric analysis (Figure 3D), we established a quantitative model of DNA synthesis in postnatal cardiomyocytes (Figures 6A to 6C). Cardiomyocyte proliferation is highest at birth, followed by a phase of multinucleation reaching a maximum around P7. The polyploidization of cardiomyocyte nuclei reflects the last wave of DNA synthesis, peaking around P14 (Figure 6B). Derivative graphs depicting the DNA content changes per time unit were calculated based on absolute quantifications of cardiomyocyte nucleus number (Figure 1C), cardiomyocyte ploidy (Figure 3D), and cardiomyocyte number (Figure 1E) without relying on markers of proliferation or the incorporation of thymidine analogs with unknown biological half-lives. As the number of cardiomyocytes and number of cardiomyocyte nuclei substantially changes postnataly, we used the time of birth as a reference for calculating postnatal DNA synthesis. Multinucleation accounted for 57% of the total postnatal DNA synthesis, cardiomyocyte number expansion was related to 30%, and polyploidization reflected 13% of this synthesis, mainly in the second and third postnatal weeks (areas under the curves, see Figure 6).

DISCUSSION

The postnatal heart has a robust capability to generate new myocardium after apical dissection and injury, although whether induced myocardiogenesis leads to complete myocardial regeneration remains controversial (Andersen et al., 2014; Jesty et al., 2012; Mahmoud et al., 2013; Sadek et al., 2014). Until recently, whether neonatal myocardiogenesis is a physiological phenomenon or whether injury is required to initiate substantial cardiomyocyte proliferation has been unknown. We demonstrated that, even in the uninjured neonatal heart, a substantial number of cardiomyocytes are generated within the first postnatal week, in agreement with the report by Naqvi et al. (Naqvi et al., 2014). However, by several distinct approaches, we failed to observe any substantial increase in the cardiomyocyte number or proliferation rate between P13 and P100.

We first used design-based stereology to establish the cardiomyocyte cell count in the left ventricle. Stereology is a powerful tool to obtain unbiased estimates of cell and nucleus numbers in different organ systems (Bergmann et al., 2015; Yeung et al., 2014). This technique relies on the accurate identification of cardiomyocyte nuclei; we and others have successfully utilized pericentriolar material 1 (PCM-1) as a specific marker for cardiomyocyte nuclei (Bergmann and Jovinge, 2012; Bergmann et al., 2011; Bergmann et al., 2015; Gilsbach et al., 2014; Preissl et al., 2015). In contrast to cell isolation strategies, stereological estimates are not dependent on isolation efficiency. Even with the most efficient method, retrograde perfusion using a Langendorff system, the expected yield of cardiomyocytes is never 100% and varies between ~1.5 and ~2.5 million in mice (older than P17) (Naqvi et al., 2014). Our cardiomyocyte number estimate is supported by previous studies that reported similar number of cardiomyocyte nuclei and cardiomyocyte nucleus density in young adult mice (Adler et al., 1996; Bersell et al., 2009). Taking our stereological estimation as a reference for the cardiomyocyte count (Figure 1E), Naqvi et al. cardiomyocyte isolation efficiency is estimated to be only 50% to 65% depending on the analyzed time points (Figures S1D and S1E). Because the amount and composition of the extracellular matrix changes dramatically in growing hearts (Anderson, 2010), it is likely that the reported cardiomyocyte increase between P15 and P17 could, at least in part, be explained by age-dependent differences in the cardiomyocyte isolation efficiencies. In this case, already changes in isolation efficiency of 15%–20% could explain the discrepancy between Naqvi et al. and our data (Figures S1D and S1E).

We performed Ki-67 staining on P14, P15, and P16 and obtained no evidence of extensive cardiomyocyte proliferation (<2% labeling frequency). By contrast, we observed that up to 13% of cardiomyocytes were in the cell cycle on P7, when most multinucleation occurs. Ki-67 expression is not restricted to mitosis but can be detected in all cell-cycle stages (G1, S, G2, and mitosis). For a cell-cycle length of approximately 24 hr (Hahn et al., 2009; Ponti et al., 2013), an extensive burst of proliferation would have been readily detected by this labeling strategy. One of the major caveats of Naqvi et al. immunohistochemistry approaches is the lack of a nuclear marker to unequivocally identify cardiomyocytes as discussed above. Without using a cardiomyocyte nuclear marker, it is difficult to distinguish cardiomyocyte from non-cardiomyocytes (Ang et al., 2010), particular in growing hearts in which the nucleus density can be more than 10-times higher than in the adult hearts (Bergmann et al., 2015). It is our impression that the provided images in Naqvi et al. do not allow an accurate discrimination between cardiomyocytes and non-cardiomyocytes being aurora B-positive (see Naqvi et al., Figures 3B, S2, and S3). Moreover, Naqvi et al. reported that approximately 30% of isolated cardiomyocytes are positive for aurora B (compared to 15% measured in tissue sections). This labeling frequency even exceeds mitotic rates in embryonic hearts by far (embryonic day 14.5: 13.9% in G2/M phase) (Walsh et al., 2010). The measured high aurora B frequency of 30% in the cardiomyocyte compartment would result in an even more dramatic increase in the number of cardiomyocytes than reported by Naqvi et al. (22% based on Langendorff preparation on P15). Given the estimated short duration of mitosis (approx. 1.8 hr in ventricular cardiomyocytes) (Mollova

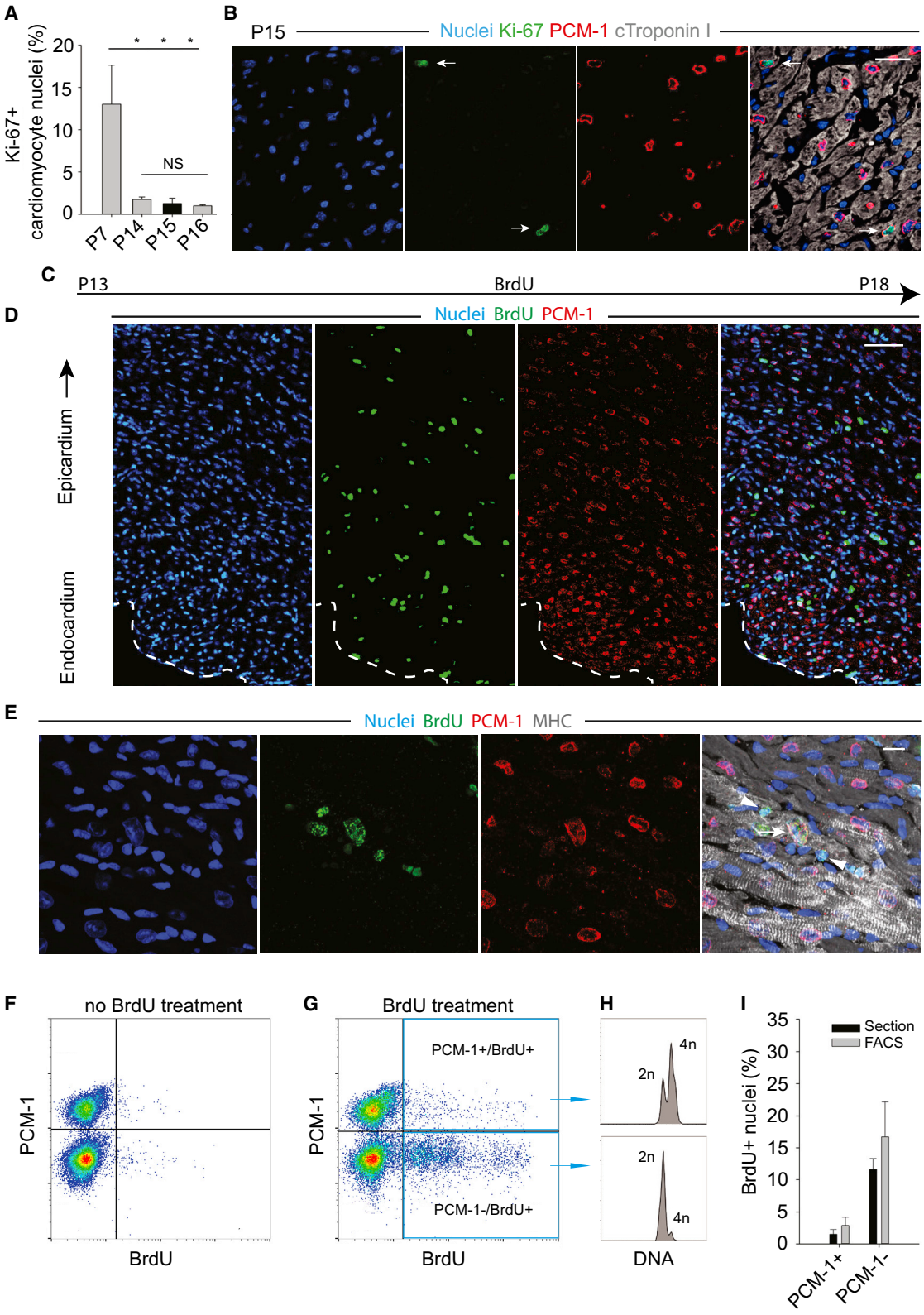

(legend on next page)

et al., 2013), 30% of mitotic cardiomyocytes in this four-hour window would translate to an expansion of the cardiomyocyte compartment by 67% (30% × 4 hr/1.8 hr). Therefore, it seems reasonable to assume that Naqvi et al. have substantially overestimated the number of aurora B-positive cardiomyocytes in their study.

One of the most prevalent techniques for detecting cell proliferation is the administration and immunohistochemical detection of thymidine analogs such as BrdU or EdU. EdU injection in the afternoon on P13 and P14 resulted in a fraction of less than 1% labeled cardiomyocyte nuclei when analyzed on P15 (Figure 2C). However, given the relatively short biological half-life of thymidine analogs, a highly synchronized proliferation of cardiomyocytes on P14 and P15 could go undetected. Therefore, we continuously administered BrdU by implanting a subcutaneous pellet on P13. In agreement with our other results, less than 3% of all cardiomyocyte nuclei had incorporated BrdU on P18 (Figure 4I), which is not compatible with the 40% increase in the cardiomyocyte cell number reported by Naqvi et al. We were also unable to confirm the regional differences in cardiomyocyte proliferation (epicardial versus endocardial regions) suggested by Naqvi et al. (Figure 4D). Furthermore, the BrdU-labeled cardiomyocyte nuclei between P13 and P18 were mainly tetraploid (Figure 4H), indicating that the majority of DNA synthesis after P13 can be attributed to polyploidization and not proliferation.

In contrast to our present study, Naqvi et al. performed a single BrdU pulse on the night of P14, which was sufficient to label a substantially larger fraction (11.3%) than detected by us of mainly diploid cardiomyocyte nuclei after a chase period of 4 days. Although, their BrdU pulse-chase experiments do not support the reported 40% increase in the cardiomyocyte cell number, their BrdU figure is still several-fold higher than in our present study. Although it is difficult to draw firm conclusions without a detailed analysis of primary data, our BrdU data obtained by both flow cytometry and by immunohistochemistry point to the possibility that Naqvi et al. cardiomyocyte nucleus isolation strategy was not rigorous enough to sufficiently remove non-cardiomyocyte nuclei from the analysis.

Because thymidine analogs (e.g., BrdU) induce the proliferation of hematopoietic stem cells (Wilson et al., 2008) and mediate toxic effects (Andersen et al., 2013), we continuously delivered biologically inert ^{15}N thymidine to detect DNA synthesis between P13 and P23 in cardiomyocytes. The labeling frequencies of cardiomyocyte nuclei were consistent with the results of our previous experiments using BrdU. Less than 3% of all cardiomyocyte nuclei incorporated ^{15}N-thymidine during preadolescence.

In the present study, we utilized rigorous strategies including design-based stereology, cell-cycle marker analysis (Ki-67), EdU pulse chase experiments, and continuous delivery of BrdU and ^{15}N thymidine. Furthermore, we analyzed cardiomyocyte proliferation both in sections and by flow cytometry without finding any evidence for a burst of proliferation or a distinct mode of cell division between P13 and P18. Instead, we observed completion of cardiomyocyte number expansion no later than P11. We further demonstrated that young cardiomyocytes exhibit multinucleation followed by polyploidization as the cells increase in size.

Cardiomyocytes lose their ability to complete the cell cycle to increase their number. This loss leads to a progressive restriction of the cardiomyocyte cell cycle in which cytokinesis is first exchanged for multinucleation, which in turn is exchanged for polyploidization. In human hearts, the pool of cardiomyocytes and the degree of multinucleation are established soon after birth (Bergmann et al., 2015; Mayhew et al., 1997), although one report has suggested that the cardiomyocyte number increases until adulthood (Mollova et al., 2013). Polyploidization occurs in both mouse and human cardiomyocytes, to different degrees. In humans, approximately 60% of all cardiomyocyte nuclei become polyploid (Bergmann et al., 2015), whereas only 10% of all cardiomyocyte nuclei become polyploid in mice. However, polyploidization occurs after multinucleation at a similar time point in both species, mostly in preadolescence. Polyploidization occurs mainly in the second and third postnatal week. Therefore it partly overlaps with Naqvi et al. suggested increase in the number of cardiomyocytes between P15–P18. However, the limited extent of polyploidization (approximately 10%) makes it unlikely that Naqvi et al. has mistaken the moderate ploidy increase for proliferation.

Given the important role of IGF-1 signaling in cardiomyocyte growth and hypertrophy (Carrasco et al., 2014; Delaughter et al., 1999), one might speculate that the T3-induced activation of the IGF-1/IGF-1-R/Akt pathway, as suggested by Naqvi et al., mainly triggers hypertrophic cardiomyocyte growth associated with polyploidization rather than cardiomyocyte proliferation in preadolescent mice.

We used the C57bl/6N mouse strain, which is a substrain to the strain (C57bl/6J) used by Naqvi et al. (Naqvi et al., 2014). A comparison of several strains, including ICR/CD1, C3Heb/FeJ, C57bl/6BRL, and C57bl/6J showed only little variation regarding the proliferative capacity and growth in the postnatal mouse

Figure 4. No Evidence for a Peak of Cardiomyocyte Proliferation in Preadolescent Mice

(A–B) Mice were sacrificed on P7, P14 (7 pm), P15 (noon), and on P16 (9.00 am). PCM-1 (red) and cardiac troponin I (gray) labeling identified cardiomyocyte nuclei (n = 3 for all analyzed time points). Cycling cardiomyocytes were identified by Ki-67 (green) expression. Arrows indicate Ki-67-positive cardiomyocyte nuclei. The black bar depicts the Ki-67 frequency on P15. The scale bar indicates 20 μm.

(C–I) BrdU was continuously delivered via subcutaneous pellets from P13 to P18 (Experimental Procedures). BrdU incorporation into cardiomyocyte nuclei (PCM-1-positive) was detected by immunohistochemistry (D, E, and I), and by flow cytometry (F to I). (D) Tile scans of a horizontal section of the mouse heart and high-magnification images (E) revealed BrdU integration into cardiomyocyte (arrows) and non-cardiomyocyte nuclei (arrowheads). Dashed lines indicate the endocardium. Scale bars: 50 μm in (D) and 10 μm in (E). (F and G) The results of flow cytometric analyses of non-BrdU-treated mice (F) and BrdU-treated mice (G). (H) Most BrdU incorporation between P13 and P18 could be detected in tetraploid cardiomyocyte nuclei, whereas most non-cardiomyocyte nuclei were diploid. The different fluorescence intensities within the BrdU-positive populations indicate different levels of BrdU incorporation. Cells may have gone through the S-phase twice after BrdU was delivered. (I) In heart sections (n = 3) and in isolated cardiac nuclei (n = 4), less than 3% of all cardiomyocyte nuclei incorporated BrdU between P13 and P18. By contrast, ~15% of all non-cardiomyocyte nuclei incorporated BrdU. * indicates $p < 0.05$.

All error bars indicate SD.

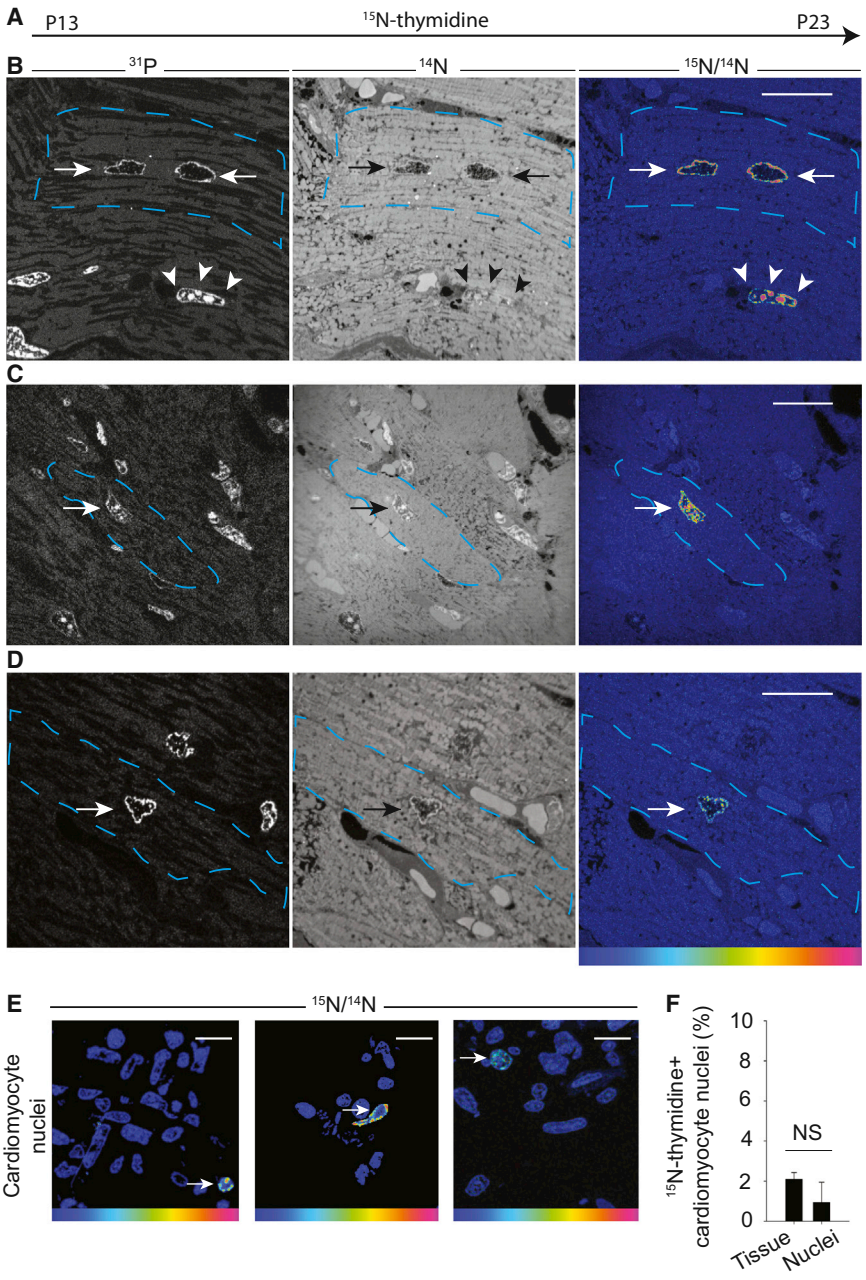

Figure 5. MIMS Analysis of ^{15}N Thymidine Incorporation in Cardiomyocytes of Preadolescent Mice

(A–E) ^{15}N-thymidine was continuously delivered via a subcutaneous pellet between P13 and P23 (Experimental Procedures). (B to D) Cardiac nuclei were identified by MIMS-based detection of ^{31}P, (left) and ^{14}N (middle). Images for ^{14}N were obtained on the species $^{12}C^{14}N^-$. The ^{14}N images reveal histological and subcellular details (cell borders and organelles) and therefore permit the identification of cardiomyocyte nuclei (arrows). $^{15}N/^{14}N$ hue-saturation-intensity images revealed an increase in the $^{15}N/^{14}N$ isotope ratios above natural abundances (blue, 0% excess; red, 300% excess) and therefore indicated ^{15}N-thymidine incorporation into cardiac nuclei (arrows). (E) ^{15}N thymidine incorporation in isolated cardiomyocyte nuclei (PCM-1 positive) by flow cytometry (as shown in Figure 3A and B). Arrows indicate cardiomyocyte nuclei with ^{15}N-thymidine incorporation.

(F) Both MIMS strategies revealed that less than 2.1% of all cardiomyocyte nuclei incorporated ^{15}N-thymidine between P13 and P23 (n = 6). Images B to D are indexed in Figure S4A. Scale bars indicate 20 μm. NS: not significant.

All error bars indicate SD.

heart (Haubner et al., 2012; Leu et al., 2001; Porrello et al., 2011; Soonpaa et al., 1996). Therefore, it is unlikely that genetic differences in the used substrains can explain the fundamental differences between our and the Naqvi et al. study.

In summary, the present study demonstrates that the mouse heart displays a robust generation of cardiomyocytes postnatally. In the uninjured neonatal mouse heart, up to 30% of all cardiomyocytes are generated even after postnatal day 2, and the full complement of cardiomyocytes (>95%) is reached after 11 days. Thus, there is a strong indication that the neonatal mouse heart harbor cues the induction of de novo myocardiogenesis to regenerate the diseased adult heart.

EXPERIMENTAL PROCEDURES

Animals

Whole litters of five to seven C57BL/6N mice with confirmed birth dates were used. Size variations between animals of the same age were minimal (the mean coefficient of variation was among all age groups 10%). Whenever possible, littermates were chosen. For the analysis of mice on postnatal day 100 only male animals were used. Mice received EdU (50 mg/kg) by subcutaneous or intraperitoneal daily injections. BrdU and ^{15}N-thymidine (euriso-top) were delivered continuously (0.5 mg/day corresponds to 60–70 mg/kg/day) to P13 mice by subcutaneously implanted pellets (Innovative Research of America, USA), which were in place for 5 and 10 days, respectively. All procedures were approved by the local ethics committee. Hearts were removed without perfusion, and the left ventricle including the septum was dissected. The wet weight of the heart and the ventricles was determined with fine scales (±0.1 mg).

Nuclei Isolation

Cardiac nuclei were isolated as described previously (Bergmann et al., 2015). Frozen heart tissue was dissected and homogenized in lysis buffer (0.32 M sucrose, 10 mM Tris-HCL [pH 8], 5 mM $CaCl_2$, 5 mM MgAc, 2 mM EDTA, 0.5 mM EGTA, 1 mM DTT) using a T-25 Ultra-Turrax probe homogenizer (IKA Germany) at 24,000 rpm for 10 s, followed by homogenization using a type A pestle in a 40 ml glass douncer (VWR) with eight strokes per sample. The nuclear isolates were filtered through 100-μm and 60-μm nylon mesh cell strainers (BD Bioscience) and centrifuged at 600 × g for 10 min. The pellets were dissolved in sucrose buffer (2.1 M sucrose, 10 mM Tris-HCl [pH 8], 5 mM MgAc). Finally, 10 ml of sucrose buffer was added to BSA-coated ultracentrifuge tubes and overlaid

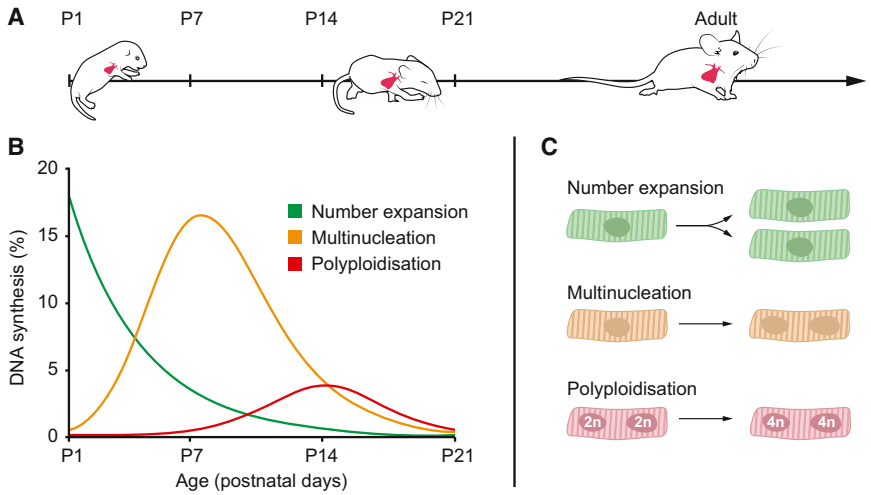

Figure 6. Cardiomyocyte DNA Synthesis in Growing Mouse Hearts

(A–C) The time course and quantification of postnatal cardiomyocyte DNA synthesis. (B and C) Cardiomyocyte proliferation, multinucleation, and polyploidization were observed in the postnatal murine heart. The magnitude and time course of the cardiomyocyte number expansion, multinucleation, and polyploidization were related. The graphs depict the DNA content changes per unit time based on stereological estimates and flow cytometric measurements of the cardiomyocyte number expansion, multinucleation, and polyploidization (Figures 1C to E and Figure 2E). The changes in DNA synthesis were related to the time around birth (P2). Diploid nuclei: 2n, tetraploid nuclei: 4n.

with the nuclear isolate. The samples were centrifuged at 13,000 × g for 60 min in a Beckman Avanti Centrifuge (Beckman Coulter), and the nuclear pellets were dissolved in NSB plus buffer (0.44 M sucrose, 10 mM Tris-HCl [pH 7.2], 70 mM KCl, 10 mM $MgCl_2$, 1.5 mM spermine). All steps were performed at 4°C.

BrdU and EdU Detection by Flow Cytometry

Nuclei were labeled with antibodies against PCM-1 (Santa Cruz, 1:200) overnight, and PCM-1 was visualized using an appropriate secondary antibody conjugated to Alexa 488 (Life Technologies). Cardiac nuclei were fixed in Fix/Perm (BD Biosciences) for 20 min on ice and sorted by flow cytometry (500,000 per tube) based on a DNA dye (Hoechst 33342). Next, the nuclei were resuspended in DNase I buffer (20 mM Tris-HCl [pH 8], 2 mM $MgCl_2$, 50 mM KCl) and incubated with 6 U of DNase I (Life Technologies) per 10^6 nuclei (37°C, 30 min). We determined that 6 U of DNase I per 10^6 nuclei is optimal for BrdU imaging of murine cardiac nuclei. The nuclei were washed once with Perm/Wash buffer (BD Biosciences) and resuspended in PBS (50 μl) for staining with BrdU antibodies conjugated to APC (BD PharMingen, 1:50, 30 min, room temperature). PCM-1 and BrdU incorporation were detected and quantified by flow cytometry. For EdU detection, we used the Click-iT EDU Alexa Fluor 647 Flow Cytometry Assay kit according to the manufacturer's instructions (Life Technologies).

MIMS Analysis

Extracted mouse tissue was minced to generate 1-mm^3 cubes and immediately fixed in 2.5% glutaraldehyde and 4% paraformaldehyde in 0.01 M PBS buffer at pH 7.2 for 2 hr at room temperature. Cardiomyocyte nuclei were isolated by flow cytometry and labeled with antibodies against PCM-1 as described in Experimental Procedures. Nuclei were transferred to 2.5% glutaraldehyde (Sigma) in 0.1 M PBS and stored in a refrigerator. Following standard electron microscopy embedding protocols, the tissue or the nuclei were post-fixed in 2% OsO_4 in PBS for 1 hr, followed by a ddH_20 wash and dehydration in an ascending alcohol series. Tissue pieces were embedded in Agar 100 resin (Agar scientific) using propylene oxide as an intermediate agent. The resin was polymerized at 60°C for 48 hr. Thin sections (150 nm) were deposited on clean silicon chips and introduced into a NanoSIMS-50 ion microprobe (CAMECA, Gennevilliers, France) operating in scanning mode (Guerquin-Kern et al., 2005). For the present study, we used a tightly focused Cs^+ primary ion beam, which allowed four secondary ion species ($^{12}C^-$, $^{12}C^{14}N^-$, $^{12}C^{15}N^-$ and $^{31}P^-$) to be monitored in parallel from the same sputtered volume. The primary beam steps over the surface of the sample to create images of the selected ion species. After careful Cs^+ ion implantation to obtain steady-state ion emission, a mosaic view of the tissue over a large area was generated using a relatively high-intensity probe with a typical spot size of 200 nm (distance between 16 and 84% peak intensity from a line scan). The raster size was 80 μm with an image definition of 256 × 256 pixels and a dwell time of 2 ms per pixel. These survey images permitted the statistical evaluation of the percentage of labeled nuclei and enabled the selection of labeled cells for further high-resolution imaging.

High-resolution images were acquired using multiframe mode. The primary beam intensity was 1 pA with a typical probe size of ~100 nm. The raster size was between 50 and 60 μm to image whole cardiomyocytes with an improved image definition of 512 × 512 pixels. With a dwell time of 2 ms per pixel, up to 20 frames were acquired, and the total analysis time was 2–3 hr. All survey images and high-resolution images were processed using ImageJ software. Before calculating local isotopic ratios, each isotopic image was properly aligned using the TOMOJ plugin (Messaoudii et al., 2007) with $^{12}C^{14}N^-$ images used as a reference before a summed image was obtained for each ion species. A ^{15}N:^{14}N ratio map was then established from $^{12}C^{14}N$ and $^{12}C^{15}N$ images based on pixel-by-pixel division. A sample containing no labeled cells was used as a working reference to adjust the detectors prior to quantification of the ^{15}N:^{14}N ratios. The final ^{15}N:^{14}N ratio map was displayed using Hue-Saturation-Intensity (HSI) transformation. These HSI color images were generated using OpenMIMS, an ImageJ plugin developed by Claude Lechene's laboratory (Lechene et al., 2006). The hue corresponds to the ratio value, and the intensity at a given hue is an index of the statistical reliability.

Stereological Analysis

Using a design-based strategy, tissue pieces (1–2 mm diameter) from the left ventricle (including the septum) were sampled. Tissues were embedded in 8% gelatin, and isectors (spheres) with a maximum diameter of 4 mm were prepared to obtain isotropic, uniform random alignment of the samples. The isectors were embedded, and 40-μm-thick cryo sections were stained for stereological quantitation. Cardiomyocyte nuclei were stained with antibodies against PCM-1, and nuclei were stained with DRAQ5 (see Immunohistochemistry). The analysis was performed on an LSM700 confocal microscope (63× Plan-Apo oil objective) using ZEN2010b software with the NewCast Module (Visiopharm A/S, version 4.x). A minimum of 3–4 isectors were sampled, and a minimum of 200 nuclei per animal were counted (1%–2% of the area of the region of interest). A systematic random sampling scheme (meander sampling) was applied using the optical dissector with a counting frame (40 μm × 40 μm × 20 μm, and 3 μm guard zones). We defined local vertical areas where myocytes had been cut along their longitudinal axis to determine the number of nuclei per myocyte. Myocyte cell borders were labeled with connexin-43 and dystrophin. Wheat germ agglutinin (WGA) was added to facilitate the identification of the cell borders in P2 and P3 animals, and myocyte nuclei were labeled with PCM-1. To estimate the total numbers of nuclei in the heart, we utilized the two-step $N_V \times V_{REF}$ method (where N_V is an estimate of the numerical cell density and V_{REF} is the reference volume of the tissue or organ region of interest) using an optical dissector (Brüel and Nyengaard, 2005). When

necessary, the tissue shrinkage along the z axis was corrected. Tissue shrinkage along the x and y axes was not observed. The total number of cardiomyocytes was calculated based on the number of cardiomyocyte nuclei and the multinucleation level.

Volume Analysis of Isolated Cardiomyocytes

We used an adaptation of the protocol reported by Mollova et al. to assess the volume of the isolate cardiomyocytes (Mollova et al., 2013). Briefly, frozen hearts were trimmed to 1-mm^3 cubes and fixed in 4% paraformaldehyde at 4°C for 2 hr, followed by washing for 2–3 hr in HBSS buffer (Ca^{2+}, Mg^{2+}). The buffer was exchanged every hour. For cardiomyocyte isolation, collagenase B (1.8 mg/ml) and collagenase D (2.4 mg/ml) (Roche) were added to the HBSS buffer (Ca^{2+}, Mg^{2+}), and the tissue pieces were incubated for 12 to 24 hr on a slow shaker at 37°C. Isolated cardiomyocytes were concentrated by spinning at 20 × g (2 min), stained with WGA conjugated to Alexa 547 (Life Technologies, 1 mg/ml, 1:500), and mounted with ProLong Gold DAPI (Life Technologies). The entire procedure beginning with the addition of the collagenase was repeated three times. Z-stack images of cardiomyocytes were obtained using a Zeiss confocal LSM 700 microscope (63× Plan-Apo oil objective), and the individual cardiomyocyte volume was measured by the Imaris 8 (Bitplane) 3D image processing software program using the surface module.

Immunohistochemistry

Mouse hearts were incubated in sucrose solution (30% Sucrose in PBS) overnight. The tissue was embedded in Tissue Tek O.C.T. Compound (Sakura) and frozen in liquid nitrogen. After cryosectioning (−25°C), 14 μm thick sections were fixed in 2% formaldehyde for 20 min. For BrdU detection, tissue sections were incubated in 2N HCl at room temperature for 40 min prior to staining, followed by extensive washing with PBS (pH 7.4). Antibodies against BrdU (Abcam, rat 1:250), Ki67-FITC (Abcam, rabbit, SP-6, 1:100), Connexin 43 (Sigma Aldrich, rabbit, 1:10,000, and Abcam, mouse, 1:200), dystrophin (Atlas Antibodies, rabbit, 1:2,000, and Abcam, mouse, 1:200), PCM-1 (Santa Cruz, rabbit 1:200), MHC (Abcam, mouse, 1:200), and cardiac troponin I (Abcam, mouse, 1:250) were used. The antibodies were visualized using appropriate secondary antibodies conjugated to Alexa 488, 555 and/or 647 (Life Technologies, 1:500). WGA conjugated to Alexa 555 and 647 (Life Technologies, 1 mg/ml, 1:500) was used to label the cell borders in P2 and P3 animals. Nuclei were visualized with DAPI or DRAQ5 (BioStatus), and sections were mounted with ProLong medium (Life Technologies). Image analysis was performed with a Zeiss LSM 700 confocal microscope using ImageJ software.

Statistics

Significant differences between continuous variables were determined by two-tailed paired and unpaired t tests and ANOVA followed by the post hoc Holm-Sidak test or by two-tailed t tests with Holm-Bonferroni correction. The data are presented as means with SD (mean ± SD). Sigma Plot 13.0 was used for statistical analysis and for dynamic fitting of the data. Derivative graphs of the cardiomyocyte number, cardiomyocyte nuclear number and ploidy levels were generated with MathCad 15.0. DNA content changes were determined compared to the level on P2. $p < 0.05$ was considered significant.

SUPPLEMENTAL INFORMATION

Supplemental Information includes four figures and can be found with this article online at http://dx.doi.org/10.1016/j.cell.2015.10.035.

AUTHOR CONTRIBUTIONS

O.B. and K.A. designed, performed, and analyzed the experiments and wrote the paper. J.P. and M.W. performed and analyzed experiments. T-D.W. and J-L.G.-K. performed the MIMS experiments. O.B. supervised the study.

ACKNOWLEDGMENTS

We thank A. Hernandez, K. Hultenby, and E. Idsund Jonsson for assistance with tissue processing for the MIMS analysis; S. Giatrellis and M. Toro for assistance with flow cytometry, and S. Jovinge and S. Zdunek for valuable discussions. This study was supported by the Swedish Research Council and the Karolinska Institutet. We acknowledge the PICT-IBiSA imaging facility at the Institut Curie for use of the ion microprobe (Nano-SIMS). O.B. was supported by the mobility program of the French Embassy in Sweden (FRÖ2014).

Received: May 6, 2015
Revised: July 30, 2015
Accepted: October 5, 2015
Published: November 5, 2015

REFERENCES

Adler, C.P. (1991). The development and regenerative potential of cardiac muscle. In The development and regenerative potential of cardiac muscle, J.O. Oberpriller, J.C. Oberpriller, and A. Mauro, eds. (London: HAP), pp. 227–252.

Adler, C.P., Friedburg, H., Herget, G.W., Neuburger, M., and Schwalb, H. (1996). Variability of cardiomyocyte DNA content, ploidy level and nuclear number in mammalian hearts. Virchows Arch. *429*, 159–164.

Ali, S.R., Hippenmeyer, S., Saadat, L.V., Luo, L., Weissman, I.L., and Ardehali, R. (2014). Existing cardiomyocytes generate cardiomyocytes at a low rate after birth in mice. Proc. Natl. Acad. Sci. USA *111*, 8850–8855.

Andersen, D.C., Skovrind, I., Christensen, M.L., Jensen, C.H., and Sheikh, S.P. (2013). Stem cell survival is severely compromised by the thymidineanalog EdU (5-ethynyl-2′-deoxyuridine), an alternative to BrdU for proliferation assays and stem cell tracing. Anal. Bioanal. Chem. *405*, 9585–9591.

Andersen, D.C., Ganesalingam, S., Jensen, C.H., and Sheikh, S.P. (2014). Do neonatal mouse hearts regenerate following heart apex resection? Stem Cell Reports *2*, 406–413.

Anderson, P.W. (2010). Myocardium and development (Paediatric Cardiology), pp. 57–72. http://dx.doi.org/10.1016/B978-0-7020-3064-2.00004-7.

Ang, K.L., Shenje, L.T., Reuter, S., Soonpaa, M.H., Rubart, M., Field, L.J., and Galiñanes, M. (2010). Limitations of conventional approaches to identify myocyte nuclei in histologic sections of the heart. Am. J. Physiol. Cell Physiol. *298*, C1603–C1609.

Bergmann, O., and Jovinge, S. (2012). Isolation of cardiomyocyte nuclei from post-mortem tissue. J. Vis. Exp. (65), 4205. http://dx.doi.org/10.3791/4205.

Bergmann, O., Bhardwaj, R.D., Bernard, S., Zdunek, S., Barnabé-Heider, F., Walsh, S., Zupicich, J., Alkass, K., Buchholz, B.A., Druid, H., et al. (2009). Evidence for cardiomyocyte renewal in humans. Science *324*, 98–102.

Bergmann, O., Zdunek, S., Alkass, K., Druid, H., Bernard, S., and Frisén, J. (2011). Identification of cardiomyocyte nuclei and assessment of ploidy for the analysis of cell turnover. Exp. Cell Res. *317*, 188–194.

Bergmann, O., Zdunek, S., Felker, A., Salehpour, M., Alkass, K., Bernard, S., Sjostrom, S.L., Szewczykowska, M., Jackowska, T., Dos Remedios, C., et al. (2015). Dynamics of Cell Generation and Turnover in the Human Heart. Cell *161*, 1566–1575. http://dx.doi.org/10.1016/j.cell.2015.05.026.

Bersell, K., Arab, S., Haring, B., and Kühn, B. (2009). Neuregulin1/ErbB4 signaling induces cardiomyocyte proliferation and repair of heart injury. Cell *138*, 257–270.

Brüel, A., and Nyengaard, J.R. (2005). Design-based stereological estimation of the total number of cardiac myocytes in histological sections. Basic Res. Cardiol. *100*, 311–319.

Carrasco, L., Cea, P., Rocco, P., Peña-Oyarzún, D., Rivera-Mejias, P., Sotomayor-Flores, C., Quiroga, C., Criollo, A., Ibarra, C., Chiong, M., and Lavandero, S. (2014). Role of heterotrimeric G protein and calcium in cardiomyocyte hypertrophy induced by IGF-1. J. Cell. Biochem. *115*, 712–720.

Delaughter, M.C., Taffet, G.E., Fiorotto, M.L., Entman, M.L., and Schwartz, R.J. (1999). Local insulin-like growth factor I expression induces physiologic, then pathologic, cardiac hypertrophy in transgenic mice. FASEB J. *13*, 1923–1929.

Gilsbach, R., Preissl, S., Grüning, B.A., Schnick, T., Burger, L., Benes, V., Würch, A., Bönisch, U., Günther, S., Backofen, R., et al. (2014). Dynamic

DNA methylation orchestrates cardiomyocyte development, maturation and disease. Nat. Commun. *5*, 5288.

Guerquin-Kern, J.L., Wu, T.D., Quintana, C., and Croisy, A. (2005). Progress in analytical imaging of the cell by dynamic secondary ion mass spectrometry (SIMS microscopy). Biochim. Biophys. Acta *1724*, 228–238.

Hahn, A.T., Jones, J.T., and Meyer, T. (2009). Quantitative analysis of cell cycle phase durations and PC12 differentiation using fluorescent biosensors. Cell Cycle *8*, 1044–1052.

Haubner, B.J., Adamowicz-Brice, M., Khadayate, S., Tiefenthaler, V., Metzler, B., Aitman, T., and Penninger, J.M. (2012). Complete cardiac regeneration in a mouse model of myocardial infarction. Aging (Albany, N.Y.) *4*, 966–977.

Herget, G.W., Neuburger, M., Plagwitz, R., and Adler, C.P. (1997). DNA content, ploidy level and number of nuclei in the human heart after myocardial infarction. Cardiovasc. Res. *36*, 45–51.

Jesty, S.A., Steffey, M.A., Lee, F.K., Breitbach, M., Hesse, M., Reining, S., Lee, J.C., Doran, R.M., Nikitin, A.Y., Fleischmann, B.K., and Kotlikoff, M.I. (2012). c-kit+ precursors support postinfarction myogenesis in the neonatal, but not adult, heart. Proc. Natl. Acad. Sci. USA *109*, 13380–13385.

Lechene, C., Hillion, F., McMahon, G., Benson, D., Kleinfeld, A.M., Kampf, J.P., Distel, D., Luyten, Y., Bonventre, J., Hentschel, D., et al. (2006). High-resolution quantitative imaging of mammalian and bacterial cells using stable isotope mass spectrometry. J. Biol. *5*, 20.

Leu, M., Ehler, E., and Perriard, J.C. (2001). Characterisation of postnatal growth of the murine heart. Anat. Embryol. (Berl.) *204*, 217–224.

Mahmoud, A.I., Kocabas, F., Muralidhar, S.A., Kimura, W., Koura, A.S., Thet, S., Porrello, E.R., and Sadek, H.A. (2013). Meis1 regulates postnatal cardiomyocyte cell cycle arrest. Nature *497*, 249–253.

Mayhew, T.M., Pharaoh, A., Austin, A., and Fagan, D.G. (1997). Stereological estimates of nuclear number in human ventricular cardiomyocytes before and after birth obtained using physical disectors. J. Anat. *191*, 107–115.

Messaoudii, C., Boudier, T., Sanchez Sorzano, C.O., and Marco, S. (2007). TomoJ: tomography software for three-dimensional reconstruction in transmission electron microscopy. BMC Bioinformatics *8*, 288.

Mollova, M., Bersell, K., Walsh, S., Savla, J., Das, L.T., Park, S.Y., Silberstein, L.E., Dos Remedios, C.G., Graham, D., Colan, S., and Kühn, B. (2013). Cardiomyocyte proliferation contributes to heart growth in young humans. Proc. Natl. Acad. Sci. USA *110*, 1446–1451.

Naqvi, N., Li, M., Calvert, J.W., Tejada, T., Lambert, J.P., Wu, J., Kesteven, S.H., Holman, S.R., Matsuda, T., Lovelock, J.D., et al. (2014). A proliferative burst during preadolescence establishes the final cardiomyocyte number. Cell *157*, 795–807.

Naqvi, N., Singh, R., Iismaa, S.E., Li, M., Calvert, J.W., Martin, D.I.K., Harvey, R.P., Graham, R.M., and Husain, A. (2015). Cardiomyocytes Replicate and their Numbers Increase in Young Hearts. Cell *163*, this issue, 783–784.

Palpant, N.J., and Murry, C.E. (2014). Proliferation at the heart of preadolescence. Cell *157*, 765–767.

Ponti, G., Obernier, K., Guinto, C., Jose, L., Bonfanti, L., and Alvarez-Buylla, A. (2013). Cell cycle and lineage progression of neural progenitors in the ventricular-subventricular zones of adult mice. Proc. Natl. Acad. Sci. USA *110*, E1045–E1054.

Porrello, E.R., Mahmoud, A.I., Simpson, E., Hill, J.A., Richardson, J.A., Olson, E.N., and Sadek, H.A. (2011). Transient regenerative potential of the neonatal mouse heart. Science *331*, 1078–1080.

Preissl, S., Schwaderer, M., Raulf, A., Hesse, M., Grüning, B.A., Köbele, C., Backofen, R., Fleischmann, B.K., Hein, L., and Gilsbach, R. (2015). Deciphering the Epigenetic Code of Cardiac Myocyte Transcription. Circ. Res. *117*, 413–423. http://dx.doi.org/10.1161/CIRCRESAHA.115.306337.

Puente, B.N., Kimura, W., Muralidhar, S.A., Moon, J., Amatruda, J.F., Phelps, K.L., Grinsfelder, D., Rothermel, B.A., Chen, R., Garcia, J.A., et al. (2014). The oxygen-rich postnatal environment induces cardiomyocyte cell-cycle arrest through DNA damage response. Cell *157*, 565–579.

Sadek, H.A., Martin, J.F., Takeuchi, J.K., Leor, J., Nie, Y., Giacca, M., and Lee, R.T. (2014). Multi-investigator letter on reproducibility of neonatal heart regeneration following apical resection. Stem Cell Reports *3*, 1.

Scholzen, T., and Gerdes, J. (2000). The Ki-67 protein: from the known and the unknown. J. Cell. Physiol. *182*, 311–322.

Senyo, S.E., Steinhauser, M.L., Pizzimenti, C.L., Yang, V.K., Cai, L., Wang, M., Wu, T.D., Guerquin-Kern, J.L., Lechene, C.P., and Lee, R.T. (2013). Mammalian heart renewal by pre-existing cardiomyocytes. Nature *493*, 433–436.

Soonpaa, M.H., and Field, L.J. (1998). Survey of studies examining mammalian cardiomyocyte DNA synthesis. Circ. Res. *83*, 15–26.

Soonpaa, M.H., Kim, K.K., Pajak, L., Franklin, M., and Field, L.J. (1996). Cardiomyocyte DNA synthesis and binucleation during murine development. Am. J. Physiol. *271*, H2183–H2189.

Soonpaa, M.H., Zebrowski, D.C., Platt, C., Rosenzweig, A., Engel, F.B., and Field, L.J. (2015). Cardiomyocyte Cell-Cycle Activity during Preadolescence. Cell *163*, this issue, 781–782.

Srsen, V., Fant, X., Heald, R., Rabouille, C., and Merdes, A. (2009). Centrosome proteins form an insoluble perinuclear matrix during muscle cell differentiation. BMC Cell Biol. *10*, 28.

Steinhauser, M.L., Bailey, A.P., Senyo, S.E., Guillermier, C., Perlstein, T.S., Gould, A.P., Lee, R.T., and Lechene, C.P. (2012). Multi-isotope imaging mass spectrometry quantifies stem cell division and metabolism. Nature *481*, 516–519.

Walsh, S., Pontén, A., Fleischmann, B.K., and Jovinge, S. (2010). Cardiomyocyte cell cycle control and growth estimation in vivo–an analysis based on cardiomyocyte nuclei. Cardiovasc. Res. *86*, 365–373.

Wilson, A., Laurenti, E., Oser, G., van der Wath, R.C., Blanco-Bose, W., Jaworski, M., Offner, S., Dunant, C.F., Eshkind, L., Bockamp, E., et al. (2008). Hematopoietic stem cells reversibly switch from dormancy to self-renewal during homeostasis and repair. Cell *135*, 1118–1129.

Yeung, M.S., Zdunek, S., Bergmann, O., Bernard, S., Salehpour, M., Alkass, K., Perl, S., Tisdale, J., Possnert, G., Brundin, L., et al. (2014). Dynamics of oligodendrocyte generation and myelination in the human brain. Cell *159*, 766–774.

Zhang, C.-H., and Kühn, B. (2014). Muscling up the heart: a preadolescent cardiomyocyte proliferation contributes to heart growth. Circ. Res. *115*, 690–692.